Applied Catalysis B: Environmental 127 (2012) 255–264

Contents lists available at SciVerse ScienceDirect

Applied Catalysis B: Environmental

journal homepage: www.elsevier.com/locate/apcatb

Low-temperature selective catalytic reduction of NO with NH_3 over V/ZrO_2 prepared by flame-assisted spray pyrolysis: Structural and catalytic properties

Thirupathi Boningari, Rajesh Koirala, Panagiotis G. Smirniotis*

Chemical Engineering Program, School of Energy, Environmental, Biological and Medicinal Engineering, University of Cincinnati, Cincinnati, OH 45221-0012, USA

ARTICLE INFO

Article history:
Received 4 April 2012
Received in revised form 4 August 2012
Accepted 16 August 2012
Available online 23 August 2012

Keywords:
Low-temperature NH_3-SCR
Vanadia (VO_x)
Zirconia (ZrO_x)
NO
Flame spray pyrolysis
In-situ FT-IR

ABSTRACT

A series of V/ZrO_2 (V/Zr atomic ratio = 0.05, 0.11, 0.17, 0.25, 0.33, 0.42), V-WO_x(0.66)/ZrO_2, and V-MoO_x(0.66)/ZrO_2 were synthesized by adopting a one-step flame spray pyrolysis technique and investigated for the low-temperature selective catalytic reduction (SCR) of NO with ammonia in the presence of excess oxygen. Our XRD results suggest that the vanadia species are in amorphous state as dominant surface monomeric VO_x species on zirconia support in V/ZrO_2 samples with $V/Zr \leq 0.17$. Further increase in vanadia content led to the formation of ZrV_2O_7 solid solution as a result of zirconia migration into the V_2O_5 crystallites. H_2-TPR data results are highly consistent with the XRD results that the low temperature shifts in the reduction peaks of 15% V/ZrO_2 catalyst attributed to the presence of more easily reducible dominant surface monomeric VO_x species. The evolution of a new reduction peak at high temperature indicates the formation of dominantly isolated polymeric V oxides species in V/ZrO_2 samples with $V/Zr \geq 0.25$. Our H_2-TPR profiles for tungsten-promoted V/ZrO_2 catalyst revealed the shift of (T_1) peak position to lower temperatures, suggesting that the reduction potential of vanadium oxide species is increased compared to V/ZrO_2 catalyst. This occurrence signifying that the addition of tungsten to V/ZrO_2 promoted the catalyst for the formation of monomeric surface vanadia species, whereas the addition of Mo promoted the formation of polymeric VO_x species and thus inhibit the SCR activity. An intense sharp band characteristic of coordinatively held NO_2 species is evident at 1630 cm^{-1}, no gaseous N_2O species were detected at 2224 cm^{-1}, 1286 cm^{-1} in the in-situ FT-IR spectra of NO adsorbed over the V/ZrO_2. Our in-situ FT-IR studies of NO+NH_3 co-adsorption demonstrate that the strong signals at 1435 and 1714 cm^{-1} (bending vibration of NH^{4+}) have seen to decrease with respect to temperature. This observation reveals that the NH^{4+} species bound to Brönsted acid sites are responsible for the enhancement in the SCR reaction over the vanadia-zirconia surfaces. The low temperature NO catalytic reduction activity would indicate that an optimal dispersion of monomeric VO_x species on zirconia is attained with the 15% of V in the V/ZrO_2 catalyst. The introduction of Zr (seven fold coordination) into V_2O_5 may lead to the reduction of elemental number in crystal grain and deviation of adjacent oxygen atoms. The change in lattice parameter, crystal anisotropy and negative thermal expansion can block the release of labile oxygen, this seems to be the reason for the decrease in catalytic activity in V/ZrO_2 catalysts with $V/Zr \geq 0.25$. The addition of tungsten has a strong influence on the NO conversion, since tungsten loading with the WO_x/VO_x atomic ratio = 0.66 exhibits a maximum conversion of ~98% in the temperature range 180–240 °C, whereas the molybdenum loading showed an inhibition effect on the SCR activity of V/ZrO_2 catalyst.

Published by Elsevier B.V.

1. Introduction

The selective catalytic reduction (SCR) of NO with NH_3 in the presence of excess oxygen at medium to high temperatures has been extensively studied mainly on V_2O_5-TiO_2 and V_2O_5(WO_x or MoO_x)/TiO_2 [1]. Many studies have investigated the activity, dispersion, the nuclearity and the oxidation state of vanadium supported on TiO_2 [2–4], $A1_2O_3$ [5,6], SiO_2 [7,8], and some of the catalysts prepared by adopting FSP method [9–11] and investigated for the high temperature SCR reaction. Although TiO_2, which is a second generation as a catalyst support after SiO_2, and $A1_2O_3$, is reducible under the reduced pressure or the reducing atmosphere, zirconia is stable under those conditions also [12]. In particular about TiO_2, catalytic performance strongly depends on its phase transformations as for example anatase is the favorable phase for SCR reaction. Unfortunately, the thermal stability and anatase content become rather poor at high temperatures. All these properties might depend on the support and it was therefore of interest to extend the study to other supports and predominantly ZrO_2. Because zirconia is very stable to thermal treatments, has

* Corresponding author. Tel.: +1 513 556 1474; fax: +1 513 556 3473.
E-mail address: panagiotis.smirniotis@uc.edu (P.G. Smirniotis).

0926-3373/$ – see front matter. Published by Elsevier B.V.
http://dx.doi.org/10.1016/j.apcatb.2012.08.012

a surface endowed with weakly acidic and basic sites, [13] and is capable to maintain a high specific surface area up to about 1000 K, if transition metal ions are present [14]. These factors allow a broad variation of the vanadia loading together with an excellent anchoring of the vanadia species on the support material.

Szakacs et al. [15] have studied the SCR activity of VO_x/ZrO_2 catalysts prepared by adsorption on ZrO_2 of $VO(acac)_2$ from toluene solutions. Indovina et al. [16] have prepared VO_x/ZrO_2 catalysts by three different conventional methods and investigated for the SCR reaction in the temperature range 473–723 K. But no FSP-based vanadium supported on ZrO_2 catalysts have been used yet for the low-temperature SCR reaction of NO with NH_3. In the past two decades flame synthesis has emerged as an eventual method for the synthesis of metal oxide nanoparticles with unique structural properties and catalytic activities. Particularly vanadium-based flame made catalysts attracted much attention due to their high activity for various reactions such as dehydrogenation of propane [17], methanol oxidation [18], methylene blue degradation [19], oxidation of butane [20], oxidative dehydrogenation of propane [21], including the SCR of NO_x at high temperatures [9–11].

In view of the increasing concerns for the synthesis of novel materials by flame aerosol technique in industry and academia, our research is focused on the development of active materials in the nanosized range to be used in selective reduction of NO with NH_3 in presence of excess O_2 at low-temperatures. Hence, the present work explores the rapid synthesis of novel vanadia-based materials via flame spray pyrolysis (FSP) for potential applications in SCR of NO with NH_3. In addition, being a single-step synthesis, high production rates, and yielding ready-to-use catalysts, FSP has other obvious advantages such as strong interactions between the highly dispersed active component and that of the functional support [12,22,23].

The main intention of our present work is not only to optimize the vanadia content for the SCR of NO reaction, but more significantly, it seeks to elucidate the structural-performance correlation of the catalyst. For every catalyst we varied the V/Zr atomic ratio used in the range of 0.05–0.42 in order to optimize the content of vanadia and to investigate the effect on SCR activity with respect to various temperatures (140–220 °C). Moreover, we investigated for the promotional effect of tungsten and molybdenum cations for the enhancement in catalytic activity and stability of the catalyst. However, the tungsten loading (W/V ratio = 0.66) has a strong influence on the NO conversion, exhibits a maximum conversion of ~98% in the temperature range 180–240 °C, whereas the molybdenum loading showed an inhibition effect on the SCR activity of V/ZrO_2 catalyst. Our in-situ FT-IR studies are evident for the direct correlation between the concentration of the Brönsted acid sites and SCR activity. The strong signals are due to the asymmetric and symmetric bending vibration mode of NH^{4+} bound to Brönsted acid sites have seen to decrease with respect to temperature. The change in lattice parameter, crystal anisotropy and negative thermal expansion can block the release of labile oxygen, this occurrence leads to the decrease in catalytic activity in V/ZrO_2 catalysts with $V/Zr \geq 0.25$.

2. Experimental

2.1. Catalysts preparation

A series of V_2O_5/ZrO_2, V_2O_5-WO_x/ZrO_2 and V_2O_5-MoO_x/ZrO_2 metal oxide nanoparticles were synthesized by a one-step FSP synthesis technique. A detailed description of the laboratory scale FSP reactor can be found elsewhere [24]. Vanadyl (V) tri-i-propoxy oxide (Strem Chemicals) was dissolved in *Ortho*-xylene (Sigma–Aldrich Reagent, 98%) with the corresponding metal precursor for the respective metal oxide support (zirconyl 2-ethylhexanoate, Strem Chemicals, ~6% Zr). Precursor solutions resulting in powders of V_2O_5-WO_x(0.66)/ZrO_2, V_2O_5-MoO_x(0.66)/ZrO_2 were prepared by dissolving pre determined amounts of tungsten (V) ethoxide (Alfa Aesar, 95%), and molybdenum 2-ethylhexanoate (Strem Chemicals, 15% Mo). The total molar concentration of V + Zr in the liquid precursor was set at the range from 0.1 to 0.5 M. During FSP, the liquid precursor was fed through a spray nozzle at a flow rate of 2 mL min^{-1} using a syringe pump (Cole Parmer, 74900 series), where it was dispersed by 5 L min^{-1} flow of O_2 (1.5 bar, Wright Brothers, 99.98%). Combustion of the dispersed droplets was ignited by a surrounding supporting flame (premixed 1.0 L min^{-1} O_2/0.85 L min^{-1} CH_4). Fine aerosol nanoparticles leaving the flame were collected on a flat glass fiber filter (Whatman GF/A, 150 mm in diameter) aided by a vacuum pump (Grainger Inc.). The aerosol nanoparticles were scraped from the filter for direct use as catalyst without any further treatment. The metal components of the catalysts are denoted as atomic ratios. The atomic ratio of the V/Zr varied for the optimization of V content to achieve high NO conversions in the SCR reaction. All the ratios of the catalysts in this study are V/Zr = 0.05, 0.11, 0.17, 0.25, 0.33, 0.42 and W or Mo/V = 0.66. For example, V-WO_x(0.66)/ZrO_2 indicates that the atomic ratio of tungsten/vanadia is 0.66.

2.2. X-ray diffraction

The powder X-ray diffraction (XRD) patterns were employed for the identification of phases of the synthesized metal oxide nanoparticles. The XRD patterns were recorded on a Phillips X'pert diffractometer using nickel-filtered Cu Kα (wavelength 0.154056 nm) radiation source and a scintillation counter detector. An aluminum holder was used to support the catalyst samples. The intensity data were collected over a 2θ range of 10–80° with a step size of 0.025° and a step time of 0.50 s. Crystalline phases were identified by comparison with the reference data from International Center for Diffraction Data (ICDD) files.

2.3. BET surface area and pore volume measurements

The BET specific surface area of the as-prepared nanoparticles was determined from nitrogen adsorption equilibrium isotherms at liquid nitrogen temperature (77 K) using an automated gas sorption system (Micromeretics ASAP 2010) operating in continuous mode. Prior to the analysis, 0.015–0.020 g of catalysts were evacuated under ultra high purity helium (UHP helium 99.999%) atmosphere for 2 h at 200 °C in the degassing port of the instrument. The adsorption isotherms of nitrogen were collected at 77 K using approximately six values or relative pressure ranging from 0.05 to 0.99 and by taking 0.162 nm^2 as the molecular area of the nitrogen molecule.

2.4. Temperature programmed reduction (H_2-TPR)

H_2-TPR of as-prepared aerosol nanoparticles was performed using an automated catalyst characterization system (Micromeritics model AutoChem 2910). Prior to the analysis approximately 0.050 g of the catalysts were pre-treated at 200 °C for 2 h in ultra high pure helium (30 mL min^{-1}) stream. A mixture of isopropanol and liquid nitrogen was used in the trapper to collect the formed water during the TPR experiment. After preheating, samples were tested by increasing the temperature from 50 to 800 °C. The temperature was then kept constant at 800 °C until the signal of hydrogen consumption returned to the initial values. The temperature programmed reduction runs were carried out with a linear heating rate (10 °C min^{-1}) in a flow of 10% H_2 in argon with a flow

rate of 20 mL min^{-1}. The hydrogen consumption was measured quantitatively by a thermal conductivity detector.

2.5. In-situ Fourier transform infrared (FT-IR) spectroscopy

In-situ infrared Fourier transform spectra were recorded using a Bio-Rad (FTS-40). The scans were collected at a scan speed of 5 kHz, resolution of 2.0, and an aperture opening of 2.0 cm^{-1}. Sixteen scans were averaged for each normalized spectrum. Circular self-supporting thin wafers (8 mm diameter) consisting of 0.006 g of material were used for the present study. The wafers were placed in a high-temperature cell with CaF_2 windows and purged in-situ in the IR cell with ultra high purity grade helium (30 mL min^{-1}, Wright Brothers) at 473 K for 2 h to remove any adsorbed impurities. Subsequently, the samples were cooled to 323 K, and the corresponding gases NH_3 (3.99% in He) or NO (2% in He) or NO + NH_3 (co-adsorption) were introduced to the cell with a flow of 30 mL min^{-1} for 1 h at 323 K to ensure complete saturation of the sample. Physisorbed gases were removed by flushing the wafer with ultra high purity helium (UHP helium 99.999%) for 3 h at 373 K. Subsequently, the in situ FT-IR spectra were recorded by desorbing gases at the respective temperatures.

2.6. NH_3-TPD

Temperature-programmed ammonia desorption data were collected on a Micromeritics Autochem 2910 Automated Catalyst Characterization System. Prior to the analysis, each sample (ca. 0.050 g) was pretreated through heating at 200 °C in an ultra high pure Helium stream (30 mL min^{-1}) with a 2 h hold. Consequently, the furnace temperature was lowered to 100 °C, and the samples were then saturated with anhydrous NH_3 (3.99% in He) at a flow rate of 30 mL min^{-1} for 1 h. The sample was flushed with 30 mL min^{-1} of ultra high purity helium (UHP helium 99.999%) for 2 h to remove weakly bound (physisorbed) NH_3, after which the sample temperature was reduced to 50 °C. Once a stable baseline by the thermal conductivity detector had been achieved, the temperature was then raised up to 800 °C at a 5 °C min^{-1} ramping rate.

2.7. Apparatus and catalytic experiments

The catalytic performance of the prepared aerosol nanoparticles in the low-temperature SCR of NO by NH_3 with excess oxygen was tested at atmospheric pressure in a continuous flow fixed bed quartz reactor. A measured amount of catalyst (0.1 g, 80–120 mesh) was placed in the reactor in between two glass wool plugs. All the gas flows were measured and calibrated using a digital flow meter (Humonics Hewlett Packard Optiflow 520). The typical reactant gas composition was as follows: 400 ppm NO, 400 ppm NH_3, 2 vol% O_2 and ultra high purified helium (UHP helium 99.999%) as balance. The premixed gases oxygen (4% in He, Wright Brothers), ammonia (3.99% in He, Wright Brothers) and nitric oxide (2.0% in He, Matheson) were used as received. The reactor was heated externally via a tubular furnace regulated by a temperature controller (Omega CN 2041), with a thermocouple inserted into the catalyst bed. The NO and NO_2 concentrations were continually monitored by a chemiluminescence NO/NO_x detector (Eco Physics CLD 70S). Prior to the catalytic experiments, the catalyst was activated in-situ by passing oxygen (4% in He, Wright Brothers) for 2 h at 200 °C temperature. The reactants and products were analyzed *on-line* using a Quadrapole mass spectrometer (MKS PPT-RGA), and a chemiluminescence NO/NO_x detector (Eco Physics CLD 70S). Reactant and product contents in the reactor effluent were recorded at 6 h of continuous reaction at each temperature step.

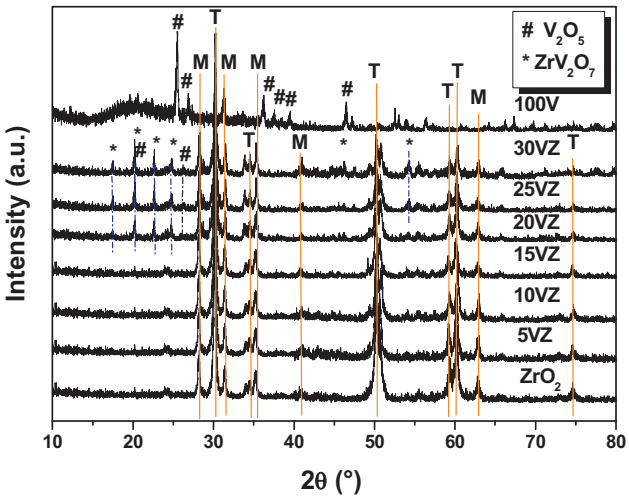

Fig. 1. Powder X-ray patterns of the FSP-made vanadia-based catalysts based on atomic ratio; M = monoclinic (ZrO_2), T = tetragonal (ZrO_2).

3. Results and discussion

3.1. Crystallite and surface characterization of V_2O_5/ZrO_2

The X-ray powder diffraction patterns of V_2O_5/ZrO_2 catalysts of various vanadia loadings synthesized by FSP method are shown in Fig. 1. For comparison purposes, diffractograms of pure V_2O_5 and pure ZrO_2 made by FSP method are also incorporated in this figure. The pure ZrO_2 sample shows sharp diffraction peaks at $2\theta = 30°$, 35°, 51°, 59.4°, 60°, 62.7 and 74.6° (JCPDS 14-534), corresponding to the presence of the tetragonal phase, and diffraction peaks at $2\theta = 28°$, 31.2°, 35.1°, 40.9° which indicates the presence of the monoclinic phase (JCPDS 36-420) [25]. No vanadium phase could be detected in any sample ≤15 wt.% vanadia, indicating that the VO_x species are in a highly amorphous state and also insertion of vanadium ions into the zirconia lattice. Crystalline V_2O_5 appears at $2\theta = 20.1°$, 26.6°, 46° (JCPDS-ICDD 9-387) when the vanadium loading increases, and ZrV_2O_7 ($2\theta = 17.4°$, 20.1°, 22.5°, 24.6°, 46.1°, 54.3° (JCPDS 16-422) formed as a result of zirconia migration into the V_2O_5 crystallites [26,27]. These results show that the XRD peaks of individual crystalline V_2O_5 or zirconium pyrovanadate (ZrV_2O_7) are absent up to the 15 wt.% loading level of vanadia. This is a clear indication that vanadium oxide species are in a highly amorphous state at low vanadia content. Addition of 20% vanadia had no effect on the particle phase of the zirconia. This indicates that the structure of ZrO_2 particles was not affected by adding V_2O_5, and that the formation of the ZrO_2 was completed before the condensation of V_2O_5 on the particle surface, in agreement with other flame-made vanadia-based catalysts [28,29]. Our XRD results suggest that the vanadia species are in surface-isolated state as dominant surface monomeric VO_x species on zirconia support in ≤15 wt.% V/ZrO_2 samples. Further increase in vanadia content led to the formation of crystalline V_2O_5 and zirconium pyrovanadate (ZrV_2O_7).

3.2. Effect of molar concentrations on textural properties, specific surface area and pore volume

The total molar concentration of the precursor solutions has significant impact on particle size and morphology [30–32]. Nanoparticles were made by FSP using wide range of molar concentration (0.1–0.5 M) of ZrO_2 precursor solutions (Fig. 2). The BET surface area and pore volume of the pure ZrO_2 monotonically increased with increasing the molar concentration and attained maximum value of 89.3 m^2 g^{-1} and 0.52 cm^3 g^{-1}, respectively at

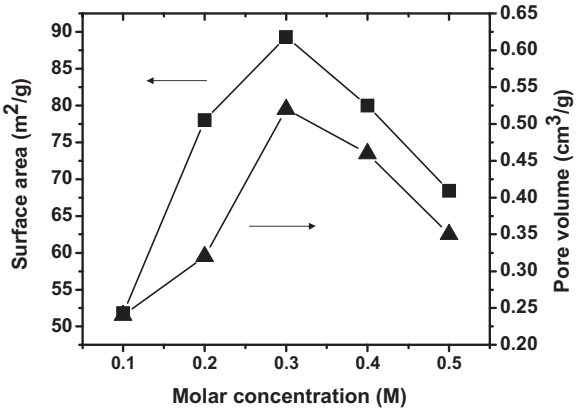

Fig. 2. Effect of molar concentration of the precursor solutions on pore volume and morphology.

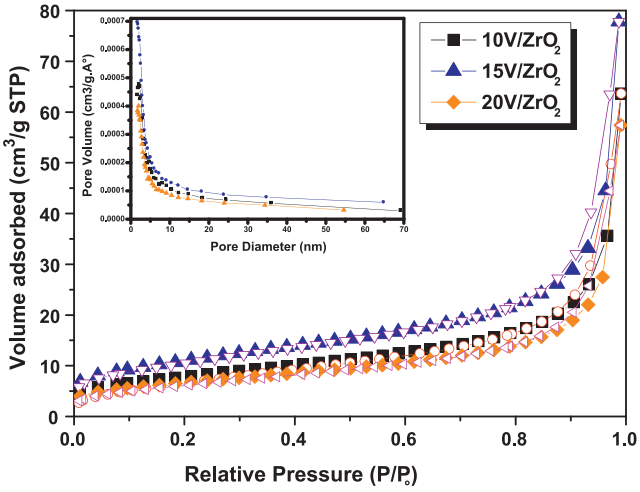

Fig. 3. Nitrogen adsorption and desorption isotherms for 10–20 V/ZrO_2 flame made catalysts. (Insert) Pore distribution of 10, 15, and 20 V/ZrO_2 samples, respectively.

0.3 M. Further increase in the total molar concentration of the precursor drastically decreased the specific surface area and pore volume of the nanoparticles. The effect of precursor molar concentration on nanoparticle physical properties is consistent with flame synthesis of SiO_2 [31] and TiO_2 [32].

The low surface area and pore volume of flame-made nanoparticles below 0.3 M due to rich fuel content within fine droplets of precursors in the reactor zone resulting sintering and agglomeration (coagulation) of the particles. Correspondingly, the resultant low surface and pore volume of flame-made nanopartilces above 0.3 M was due to the increase in concentration of the precursor droplets with the provided residence time in the flame-reaction zone leading to higher particle collisions resulting in particle diameter growth, which reduced the surface area of the material especially when coalescence takes place. Similar observations also made with the flame-made materials in the literature [33,34]. For this reason, the catalysts for SCR experiments were synthesized using 0.3 M precursor solution with 2 mL min^{-1} of feed flow rate and 5 L min^{-1} of O_2 dispersion gas.

A series of vanadia-zirconia nanoparticles (V/ZrO_2) were synthesized rapidly in a direct flame spray pyrolysis using 0.3 M precursor solution, showing composition dependent porevolume and specific surface areas of 0.04–0.52 $cm^3\ g^{-1}$, 68–88 $m^2\ g^{-1}$, respectively (Table 1). In the absence of vanadia content, i.e. 0VZ, showed high specific surface area and porevolume. As expected, there is a little inverse relation between BET surface area and vanadium content. It is because the surface vanadium oxide species have been described to destabilize the texture of the support [35,36]. There is a minimal decrease in SSA and porevolume of the vanadia samples up to 20% (w/w). It can be seen that the porevolume and surface area were drastically dropped to 0.04 $cm^3\ g^{-1}$ and 14 $m^2\ g^{-1}$, respectively with further increase in V content in the sample.

We have investigated the N_2 adsorption/desorption isotherm studies for the selected flame made samples (10–20 V/ZrO_2). The representative results are now shown in Fig. 3. One can observe from the figure that the 15 V/ZrO_2 catalyst undergo to the monotonical increase in the adsorbed volume at a high relative pressure and followed by plateau, which is in turn a characteristic of solid microporous [37]. Whereas, comparatively low adsorption was observed in 10 V/ZrO_2 and 20 V/ZrO_2 samples. The hysteresis presented at high relative pressure as the Type II isotherms, in 15 V/ZrO_2 indicates the presence of mesopores. The adsorption/desorption isotherms results for 10 V/ZrO_2 and 20 V/ZrO_2 samples suggest that the adsorbed volume for both samples at the middle of relative pressure is very similar. However, 15 V/ZrO_2 adsorption/desorption isotherms are highly significant at low and high relative pressures. The 15 V/ZrO_2 catalyst showed an adsorption–desorption hysteresis cycle which can be attributed to capillary condensation in mesoporous solids. Our FSP vanadia-based materials showed an identical adsorption/desorptions, these results illustrate that the differentiation could not be found between internal pores and external pores and they are highly homogeneous.

3.3. Temperature-programmed reduction (H_2-TPR)

In the present study, the reducibility of V/ZrO_2 samples was investigated by the deconvoluted quantitative H_2-TPR (Fig. 4, Table 2) to ensure the oxidation states of different loadings of vanadium oxide deposited on the zirconia and relate these oxidation states with the SCR activity studies of the catalysts. Three distinctive reduction peaks at 863 K (T_1), 927 K (T_2) and 1010 K (T_3) were evident in the deconvoluted TPR profile for the pure vanadia sample (Table 2). A similar observation has been reported in the literature [38–40]. As one can observe in Fig. 4, the two reduction peaks (T_1

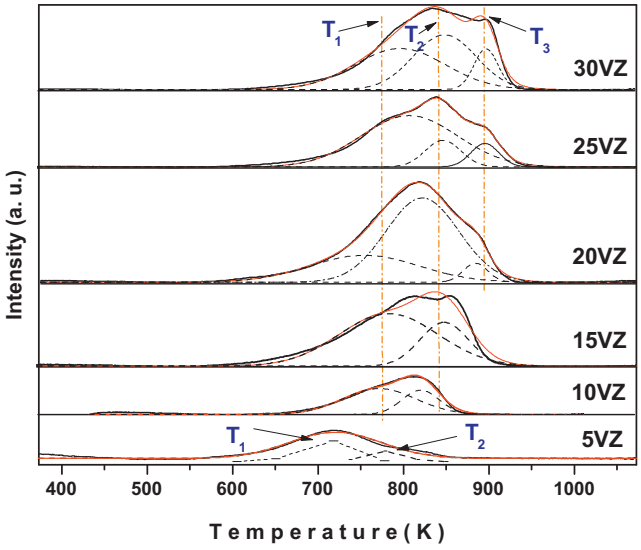

Fig. 4. H_2-TPR patterns of X-V_2O_5/ZrO_2 (X = 0.05, 0.11, 0.17, 0.25, 0.33, 0.42); X = V/Zr atomic ratio; evolution of new reduction peak at high-temperatures in X-V_2O_5/ZrO_2 (x = 0.25, 0.33, 0.42) catalysts.

Table 1
Scherrer-determined crystallite size, specific surface area and pore volume of V/ZrO_2 as a function of increasing V_2O_5 content.

Flame-Made Catalyst	XRD phases	S_{BET} ($m^2\ g^{-1}$)	Pore diameter (nm)	Pore volume ($cm^3\ g^{-1}$)
ZrO_2	T, M	89.2	01.2	0.52
5 V/ZrO_2	T, M	31.9	19.3	0.13
10 V/ZrO_2	T, M	26.9	14.2	0.12
15 V/ZrO_2	T, M	22	14.4	0.11
20 V/ZrO_2	ZrV_2O_7, V_2O_5, T, M	21	15.2	0.09
25 V/ZrO_2	ZrV_2O_7, V_2O_5, T, M	14	09.7	0.03
30 V/ZrO_2	ZrV_2O_7, V_2O_5, T, M	12	07.2	0.04
15 V-WO_x(0.66)/ZrO_2[a]	T, M	21.6	10.5	0.07
15 V-MoO_x(0.66)/ZrO_2[b]	T, M	13.4	06.1	0.02
100 V	V_2O_5	14.5	9.95	0.03

T – tetragonal (ZrO_2); M – monoclinic (ZrO_2).
[a] W/V atomic ratio = 0.66.
[b] Mo/V atomic ratio = 0.66.

Table 2
H_2-temperature programmed reduction and hydrogen consumption of as-prepared catalysts V-based samples.

Catalyst	T (K)			H_2 consumption (μmol g^{-1})
	T_1	T_2	T_3	
ZrO_2	916	1017	–	237
5 V/ZrO_2	717	781	–	1097
10 V/ZrO_2	770	823	–	2750
15 V/ZrO_2	776	847	–	4418
20 V/ZrO_2	760	821	884	7821
25 V/ZrO_2	805	848	896	8438
30 V/ZrO_2	803	848	900	10,315
15 V-WO_x(0.66)/ZrO_2	760	848	1058 (WO_x)	15,282
15 V-MoO_x(0.66)/ZrO_2	783	822	994 (MoO_x)	6378
V_2O_5	863	927	1010	7133

and T_2) were overlapped in the H_2-TPR profile of 5% V/ZrO_2 catalyst. As the vanadia content increased to 20%, a new high temperature peak (T_3) appeared to merge. Hence, it is highly difficult to distinguish the specific oxidation state of vanadia species without peak deconvolution. To better understand the oxidation states of vanadia and quantitative hydrogen consumption, the overlapped reduction peaks were deconvoluted into sub-bands by searching for the optimal combination of Gaussian bands. The selection of number and shape of the peaks to be fitted to each of the original profiles was not arbitrary. The temperatures corresponding to these peaks are listed in Table 2.

For the pure V_2O_5, three distinctive peaks from 863 to 1010 K with temperature of reduction rate maximum (T_{max}) at 1010 K are ascribed to the stepwise reduction of the vanadium oxide from V^{5+} to V^{4+} [38], At low V loadings ($\leq$15%) the catalysts exhibit a reduction peak depending on vanadium content in catalysts and the reduction initiates between 717 and 847 K. This low temperature shifts in the reduction peaks can be attributed to the presence of more easily reducible highly isolated dominant surface monomeric VO_x species. With increasing V coverage, reduction temperatures shifted to high temperatures and a new reduction peak was appeared in the range of 886–896 K for the (20–30%) V/ZrO_2 samples, indicating lower reducibility of the high-coverage VO_x species. The evolution of a new reduction peak at high temperature indicates the formation of dominantly isolated polymeric V oxides species [41]. Hence, we consider any significant shift to higher reduction temperatures at increasing vanadia loadings as suggestive of a structural difference in the surface VO_x species. These results are in consistent with the XRD patterns, where the formation of zirconium pyrovanadate (ZrV_2O_7) initiated from the 20% V/ZrO_2 as a result of zirconia migration into the V_2O_5 crystallites [26,27]. On the one hand, it is a fact that the ionic radius of V^{5+} (0.065 nm) are smaller than that of Zr^{4+} (0.079 nm), so it is easier for V^{5+} to incorporate into ZrO_2 lattice to generate zirconium pyrovanadate (ZrV_2O_7) solid solution.

The hydrogen-TPR profiles of 15% V/ZrO_2 and 15% V-WO_x (MoO_x)/ZrO_2 as-prepared catalysts were also recorded (Fig. 5) to investigate the promoting effect of tungsten and molybdenum on V/ZrO_2 samples for the SCR reaction. As shown in Fig. 5, there

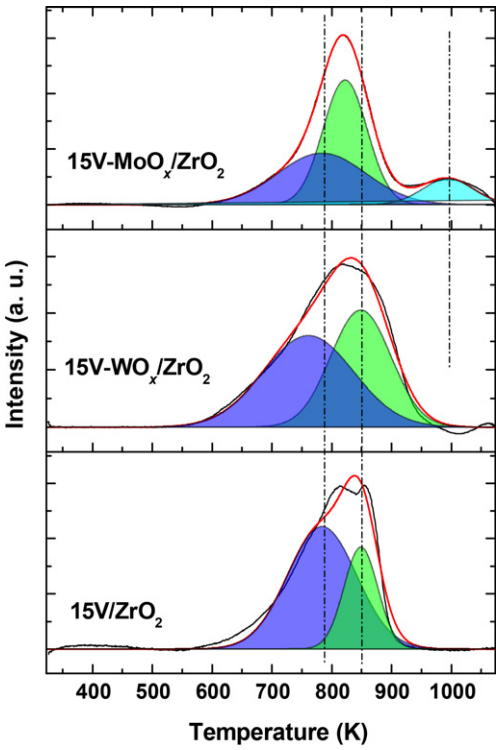

Fig. 5. H_2-TPR profiles of V/ZrO_2 and V-WO_x(MoO_x)/ZrO_2 samples; promoting effect of tungsten.

Table 3
Lewis, Brönsted acid peak areas and total acidity for the catalysts involved in the present study during the ammonia desorption (temperature programmed ammonia desorption).

Catalyst	Physisorption (%)[a]	LA (%)[a]	BA (%)[a]	Total acidic site distribution (%)[a]
ZrO_2	9.9↓	84	5	90
5 V/ZrO_2	18.7	54	27	81
10 V/ZrO_2	12.3	56	31	87
15 V/ZrO_2	0.2	43	56	99
20 V/ZrO_2	18.7↑	27	54	81
25 V/ZrO_2	19.3	28	52	80
30 V/ZrO_2	60.2	27	12	39

[a] Peaks were deconvoluted using the Gaussian function.

were only two deconvoluted reduction peaks (T_1, T_2) observed for the 15 wt.% V/ZrO_2 catalyst, which demonstrate the formation of an oxide in which vanadium has an oxidation state between V^{+5} and V^{+4}. The low temperature reduction peak (T_1) in the TPR profile of 15% V/ZrO_2 should be assigned to surface species, which is due to subsistence of surface monomeric VO_x species. The H_2-TPR results for tungsten-promoted V/ZrO_2 catalyst showed the shift of (T_1) peak position to lower temperatures, suggesting that the reduction potential of vanadium oxide species is increased compared to V/ZrO_2 catalyst (Fig. 5). This occurrence suggesting that the addition of tungsten promoted the catalyst for the formation of monomeric surface vanadia species. No strong peak was observed for the reduction of tungsten species in V-WO_x/ZrO_2, but one strong peak at 994 K was observed for the reduction of surface molybdenum species in V-MoO_x/ZrO_2 catalyst. These results are in highly agreement with the SCR activity results, where the addition of WO_x promoted the catalytic activity for high NO conversion whereas the addition of MoO_x inhibited the SCR activity. The NO conversion decreased drastically with the addition of molybdenum content to the V/ZrO_2 catalyst, which may be caused by the blocking effect of the surface active pores by the loading of molybdenum oxide. Quantitative hydrogen consumption analysis shows that the reducibility of the vanadia species (H_2 consumption) also greatly improved by the addition of tungsten, whereas no improvement of the reducibility observed for V-MoO_x/ZrO_2 catalysts (Table 2). Enhancement in the reduction potential of vanadia species and surface-isolated state of surface monomeric VO_x species seem to be the reason for high SCR activity of V-WO_x(0.66)/ZrO_2 catalyst.

3.4. Acidic sites distribution (NH_3-TPD)

Beside the oxidation state of V species, acidic sites distribution of the catalyst and their quantities are equally important characteristics in the SCR of NO. The acidic sites distribution of the as-prepared V/ZrO_2 catalysts with various V loading was determined using ammonia TPD technique (Fig. 6, Table 3). The NH_3-TPD profiles show that the bulk ZrO_2 synthesized by FSP possesses only weak surface Lewis acid sites with no apparent surface Brönsted acid sites. The number of surface Lewis acid sites slightly increase and the distribution of surface Brönsted acid sites monotonically increase as the V content increase up to 15% in the catalyst. Further increase in the V loading, decreases the distribution of strong acidic sites. From Fig. 6, one can observe the increase of ammonia physisorption (at 466 K) for the catalysts containing high V amounts. This phenomenon clearly indicates the interaction between ZrO_2 and vanadia becomes feeble and thus, the formation of dominant surface isolated tetrahedral VO_x species with different oxygen environments. This occurrence was also established by our XRD and TPR results as we demonstrated above. In the present NH_3-TPD study, broad and strong acid site distribution is observed for the 15 V/ZrO_2 catalyst. Our TPD studies suggest that the doping of ZrO_2 with 15 wt.% vanadia can remarkably improve the concentration and distribution of the surface strong acidic sites.

3.5. Low-temperature catalytic reduction of NO by NH_3 over V/ZrO_2

Initially, we evaluated the potential catalytic performance of a series of as-prepared V/ZrO_2 catalysts with respect to the temperature (160–220 °C) in the SCR of NO with ammonia to optimize the V content and to ensure the influence of high V content on NO conversion. In each experiment, a series of V/ZrO_2 samples were used to study the effect of vanadia loading as a function of V weight ratio with respect to the temperature. Prior to the catalytic performance tests, a reaction with as-prepared ZrO_2 sample was performed at 220 °C to test the catalytic activity of the ZrO_2 and the efficiency of SCR unit. In the absence of V, the NO conversions were very low (≤12%) when only ZrO_2 was used as catalyst (not shown in Fig. 7) at relevant conditions.

An enhancement of the NO conversion was observed over ZrO_2 with the addition of 5% V, resulting in an initiation at 140 °C and reaching a value of 35% at 200 °C but, does not accomplish high NO conversions. Improvement in NO conversion is further evident with the addition of 15% V. As the V content increases up to 15% on the ZrO_2, the NO conversions increased monotonically and reached a maximum value of 76% at 200 and 220 °C. Further increase in the V content (20% V/ZrO_2-30% V/ZrO_2) drastically decreased the NO conversions and stability. This would indicate that an optimal dispersion of monomeric VO_x species on zirconia is attained with this amount of V in the 15% V/ZrO_2 catalyst. These NO catalytic reduction activity performances of the as-prepared V/ZrO_2 catalysts are in highly agreement with the XRD results, where the ZrV_2O_7 formed as a result of zirconia migration into the V_2O_5 crystallites upon increase in the V content. The introduction of Zr (seven fold coordination) into V_2O_5 may lead to the reduction of elemental number in crystal grain and deviation of adjacent oxygen atoms. In the case of ZrV_2O_7, the number of adjacent oxygen coordination around V decreases substantially and results in the formation of new structure, the change in lattice parameter and crystal anisotropy may block the release of labile oxygen, this occurrence leads to the decrease in catalytic activity.

The ZrV_2O_7 is structurally associated to ZrW_2O_8. It shows negative thermal expansion at temperatures above 102 °C. Below this temperature it undergoes phase transitions to an incommensurate structure, and then to a $3 \times 3 \times 3$ cubic superstructure [42,43]. The superstructure contains 108 octahedra and 216 tetrahedra in each unit cell. These units can be arranged by various ways in the structure. This degeneracy is thought to be linked to the unusual thermal expansion properties of zirconium pyrovanadate (ZrV_2O_7). The simple cubic cell with ZrO_6 octahedra and VO_4 tetrahedra is shown in Fig. 8 [42,43]. Moreover, it is evident from our XRD studies that the formation of crystalline V_2O_5 and ZrV_2O_7 commence from the 20% V/ZrO_2. It has been revealed that the release of the structural distortion upon the successive phase transitions with large volume increase leads to the negative thermal expansion of ZrV_2O_7 at above 100 °C [44]. This might be the main cause for the decrease in SCR activity of as-prepared 20–30 wt.%V/ZrO_2 catalysts.

The results presented in Fig. 7 indicate that an optimal dispersion of monomeric VO_x species on zirconia is attained with the amount of 15% V on ZrO_2 support for the high conversion of SCR reaction at low-temperatures. However, the NO conversion does not accomplish 100% even with the 15 wt.% V/ZrO_2. We have doped V/ZrO_2 catalyst with the tungsten cations and molybdenum cations independently, to ensure about the promotion effect on the SCR reaction at low-temperatures. Fig. 9 shows the NO conversion as a function of dopant (WO_x, MoO_x) with respect to the temperature range (140–260 °C) in the NH_3-SCR reaction over 15 V-(WO_x)

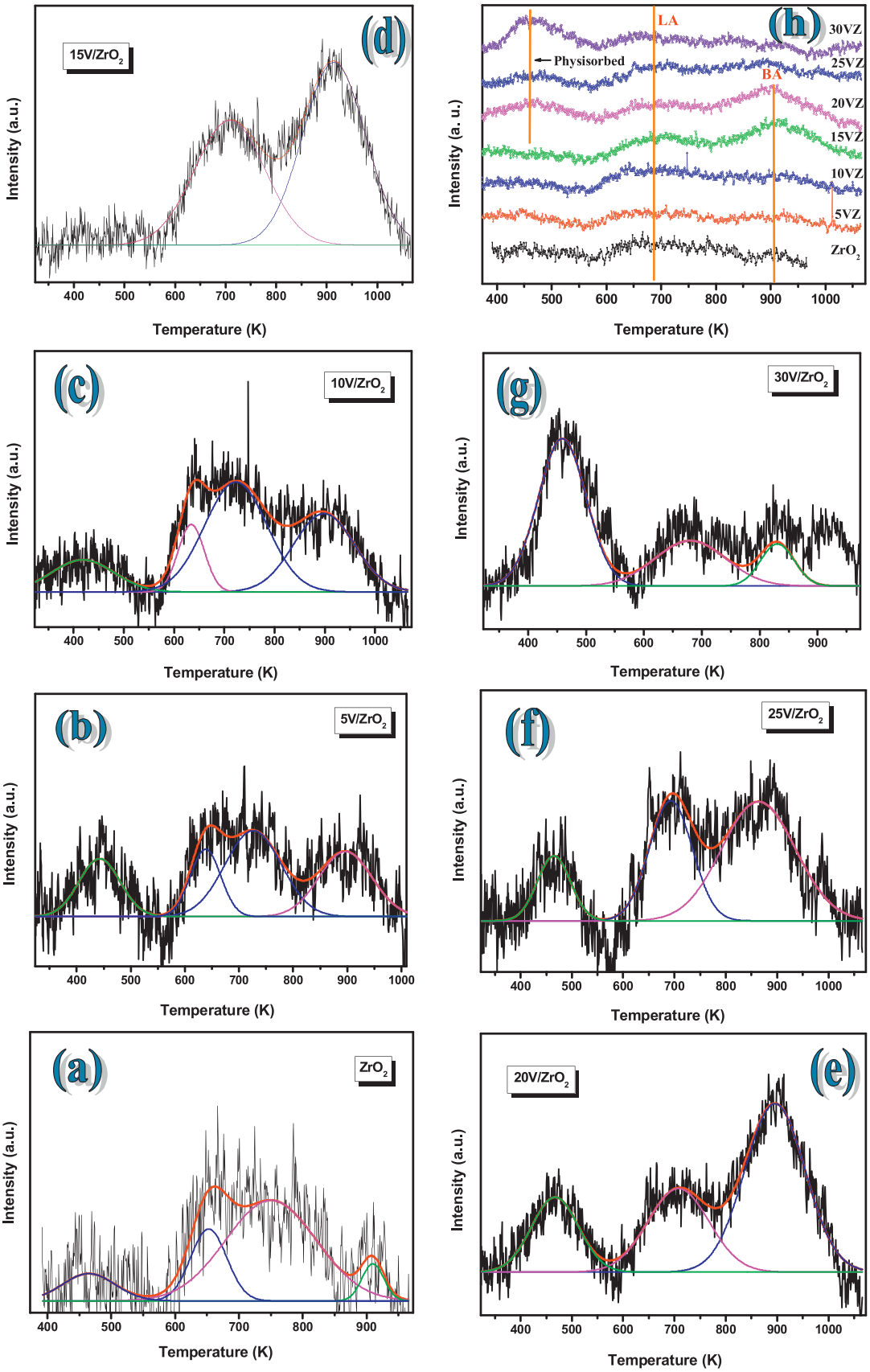

Fig. 6. De-convoluted NH_3-TPD patterns of as-prepared (a) ZrO_2, (b) 5 V/ZrO_2, (c) 10 V/ZrO_2, (d) 15 V/ZrO_2, (e) 20 V/ZrO_2, (f) 25 V/ZrO_2, (g) 30 V/ZrO_2, and (h) all the V/ZrO_2 samples together for comparison.

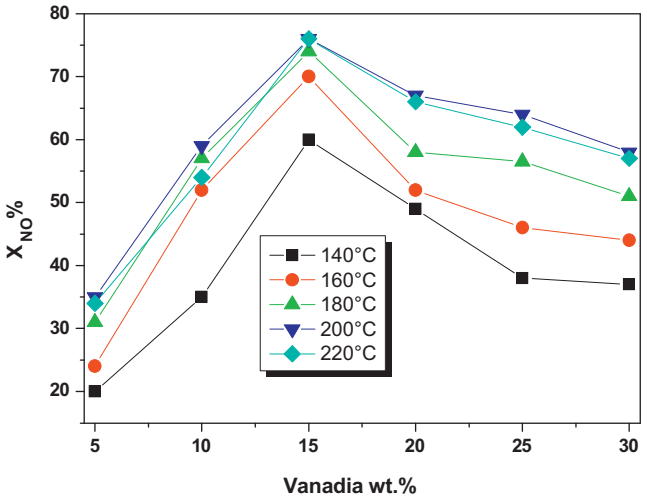

Fig. 7. Influence of V/Zr atomic ratio on NO conversion in the SCR reaction of (0.05–0.42)V/ZrO_2 catalysts as a function of V content with respect to the temperature; GHSV = 24,000 h^{-1}; feed: NO = 400 ppm, NH_3 = 400 ppm, O_2 = 2 vol.%, He carrier gas, X_{NO}% = conversion of NO at 6 h on stream.

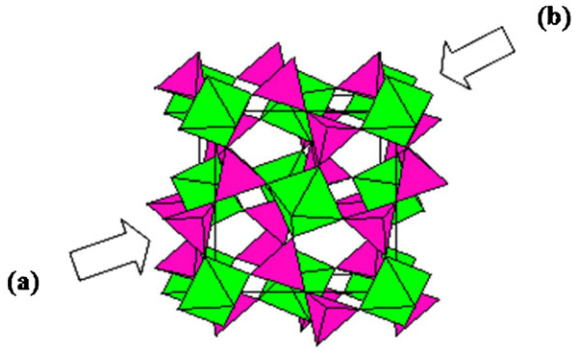

Fig. 8. Plausible crystal structure of zirconium pyrovanadate (ZrV_2O_7): (a) ZrO_6 octahedra and (b) VO_4 tetrahedra.

or $(MoO_x)/ZrO_2$ catalysts. The tungsten loading has a strong influence (promotional effect) on the NO conversion, since tungsten loading with the WO_x/VO_x ratio = 0.66 exhibits a maximum conversion of ~98% in the temperature range 180–240 °C, whereas

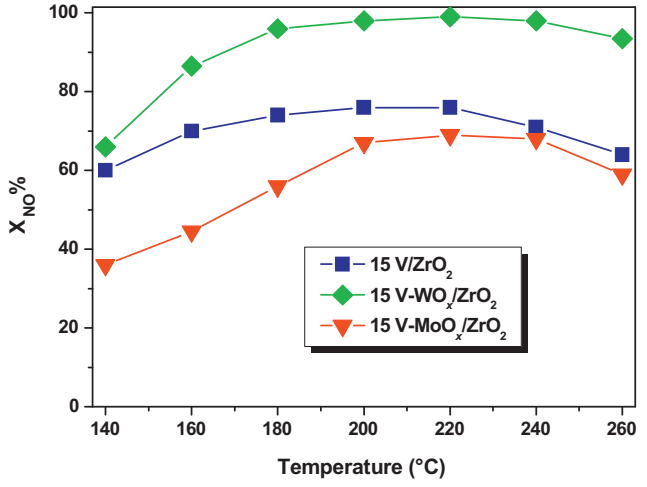

Fig. 9. Impact of WO_x and MoO_x on NO conversion in the SCR reaction at different temperatures over V/ZrO_2 catalysts; GHSV = 24,000 h^{-1}; feed: NO = 400 ppm, NH_3 = 400 ppm, O_2 = 2 vol.%, He carrier gas, X_{NO}% = conversion of NO at 6 h on stream.

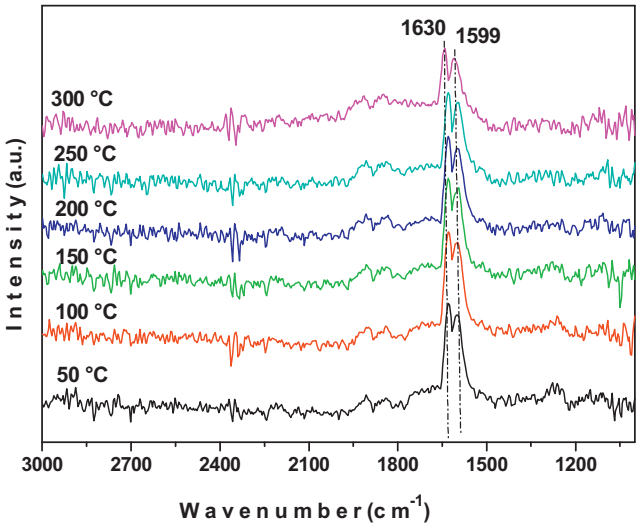

Fig. 10. In-situ FT-IR spectra of coordinatively held NO species, adsorbed at 323 K over the 0.17 V/ZrO_2 catalyst and successively increasing temperatures up to 573 K.

the molybdenum loading showed an inhibition effect on the SCR activity of V/ZrO_2 catalyst (Fig. 9). These SCR activity results are in highly agreement with the H_2-consumption results which are associated to the surface dispersion of vanadia species on zirconia. The hydrogen-consumption (μ mol g^{-1}) value increased monotonically for the 15 V-WO_x/ZrO_2 catalyst, whereas these values drastically decreased for the 15 V-MoO_x/ZrO_2 catalyst.

3.6. *In-situ Fourier transform infrared (FT-IR) spectroscopy*

We did not observe any NO absorption peaks over the surface of as-prepared V/ZrO_2 sample. These observations are in agreement with those reported in the literature [41,45]. This adsorption behavior is not surprising since it has been observed in many instances that NO adsorption occurs on reduced oxide surfaces [46,47]. Also, the (d^0) configuration of the V^{5+} ions does not allow the accommodation of the antibonding electron in the NO molecule upon chemisorptions. These results show that NO does not chemisorb over the vanadia surface. In order, to acquire the information about the presence of weakly adsorbed species, we have recorded this spectrum during the in-situ adsorption of NO over the vanadia-zirconia catalyst with respect to the temperature (Fig. 10) without flushing the wafer with ultra high purified helium.

From Fig. 10, an intense sharp band characteristic of coordinatively held NO_2 species is evident at 1630 with a shoulder at 1599 cm^{-1} absorption peaks [48–50]. Intensity of the 1630 and 1599 cm^{-1} peaks was decreased in the spectrum obtained during the evacuation at 573 K, indicating that the adsorbed NO gas species are removed. No gaseous N_2O species were detected at 2224 cm^{-1}, 1286 cm^{-1} over the surface of vanadia-zirconia [51]. We did not observe the formation of monodentate nitrate species at 1451 cm^{-1} and $(NO_3^-)_2$ species at 1380 cm^{-1} [52] over the surface of as-synthesized V/ZrO_2 catalyst.

Fig. 11 shows the IR spectra of ammonia adsorbed on 15 wt.% V/ZrO_2. On the sample, a distinct bands at 1602, 1613, 1668, 1714, 1736 and 2341 cm^{-1} are observed. The 1668 cm^{-1} band is attributed to the symmetric bending vibration of NH^{4+} [51,53]. It is distinguished that the ν_s NH^{4+} peak is shifted upward at 100 and 150 °C due to the chemisorption and strong co-ordination [54], extent of such a shift being a measure of the weakening of coordination bond [55]. Consequently, at 200 °C a new peak evolved at 1602 cm^{-1} which is attributed to δ_{as} (NH_3) coordinated to Lewis acid sites [56,57]. 3243 cm^{-1} peak ascribed to Fermi resonance of

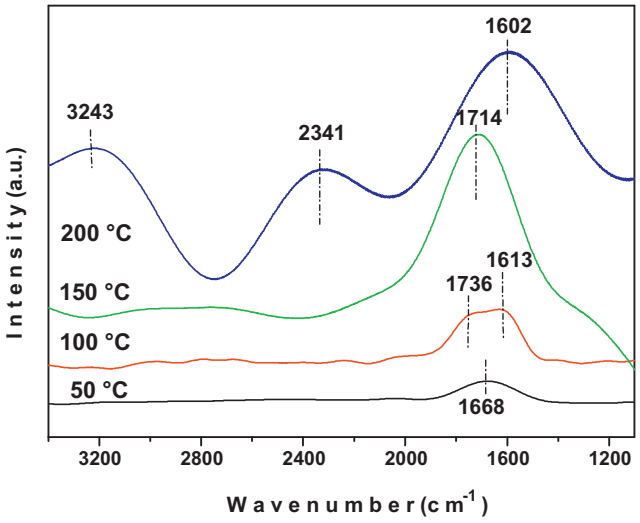

Fig. 11. In-situ FT-IR spectra of the adsorbed species over the 0.17 V/ZrO_2 catalyst, arising from contact of ammonia and degassed at various temperatures (323–523 K).

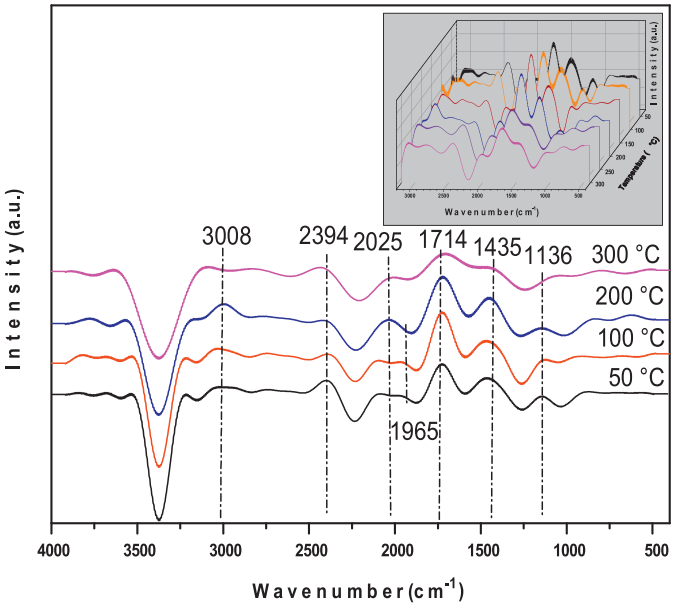

Fig. 12. In-situ FT-IR spectra of NH_3 + NO co-adsorption over the 0.17 V/ZrO_2 catalyst at 323 K and further outgassing at different temperatures (50–300 °C); inside rectangle: a progressive disappearance of the adsorbed NH_3 + NO bands during the evacuation increasing temperatures.

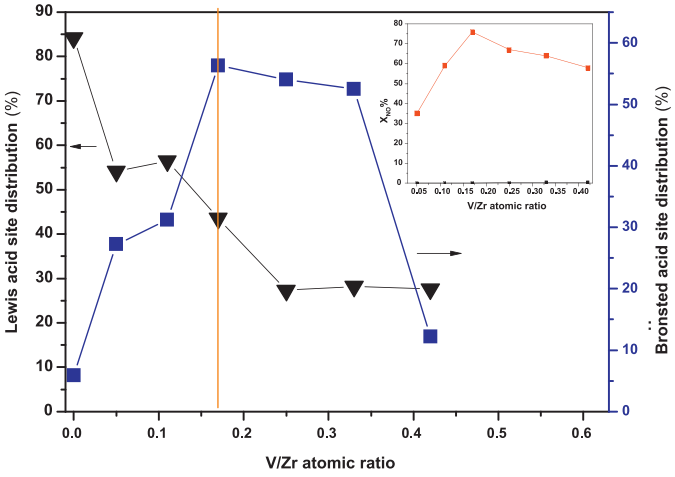

Fig. 13. Direct correlation between the concentration of the Brönsted acid sites and SCR activity of V/ZrO_2 as-prepared catalysts.

ν_{as} NH_3 and ν_s NH_3 and is assigned to chemisorbed ammonia [51]. The absorption peak at 1428 cm^{-1} is absent which is high intense peak and ascribed to Brönsted acid sites bound δ_{as} (NH_4^+) vibrations over the V_2O_5/TiO_2 samples [4,51,53]. This occurrence suggesting that the zirconia supported vanadia samples follow different reaction pathway. These results are in agreement with the literature reports, where the NH^{4+} species did not form on V_2O_5-ZrO_2 samples with V-content lower than 1.5 atoms nm^{-2} [16]. These results are suggesting that both Brönsted acid sites (associated with V-OH surface groups) and Lewis acid sites are present over the vanadia-zirconia aerogel surfaces.

Earlier studies on V_2O_5-based catalysts [58] have shown that, of the reactants NH_3 and NO, only NH_3 is strongly adsorbed. Thus, one can get insight regarding the nature of the SCR reaction by exposing a catalyst with the co-adsorption of NH_3 and NO. The in-situ FT-IR spectra of NH_3 + NO co-adsorbed over the 15 V/ZrO_2 aerogel catalyst at 323 K and evacuation at successive temperatures (Fig. 12) exhibit dominant peaks at 1435 and 1714 cm^{-1}. The peak at 1435 cm^{-1} is assigned to the ν_4 (F) bending mode of Brönsted acid sites bound ammonium ions [49,51,53], but the corresponding ν_2 (E) vibration mode is absent at 1660 cm^{-1} [59]. It has been established in the literature that there is a direct correlation between the concentration of the Brönsted acid sites and SCR activity. Inconsistence, our in-situ FT-IR studies also show that the NO conversion is directly correlated to the concentration of the Brönsted acid sites (as indicated by the intensity of the peaks at 1435 and 1714 cm^{-1} in Fig. 12). The strong signals are due to the asymmetric and symmetric bending vibration mode of NH^{4+} bound to Brönsted acid sites (in particular the signals at 1435 and 1714 cm^{-1}) have seen to decrease with respect to temperature (Fig. 12). This observation reveals that the NH^{4+} species bound to Brönsted acid sites are responsible for the enhancement in the SCR reaction over the vanadia-zirconia surfaces. The symmetric bending vibration mode of NH^{4+} has to appear at around 1668 cm^{-1} [51,53], this peak is shifted to high wavenumber (1714 cm^{-1}) due to the strong co-ordination or chemisorption. Our in-situ FT-IR results are in highly agreement with the ammonia temperature programmed desorption experimental results where the direct correlation between the concentration of the Brönsted acid sites and SCR activity found (Fig. 13).

The absorption band with a maximum at 2025 cm^{-1} and a shoulder at approximately 1965 cm^{-1} is attributed to the nitrate bands, they are assigned to two types of V-NO nitrosyls species, which contain NO_3^- ions in their coordination spheres (i.e. (ON)–V^{n+}–(ONO_2^-) complexes). Our in-situ FT-IR results (Fig. 12) suggest that the nitrosyls at 1965 cm^{-1} are least stable species at above 373 K [60]. The broad band region around 3000 cm^{-1} can be ascribed to the hydrogen bonding between NH_3 and catalyst surface. The absorption peak at 1136 cm^{-1} is corresponding to the chelating bidentate nitrites [61].

4. Conclusions

In this work, a series of novel V/ZrO_2 (V/Zr atomic ratio = 0.05, 0.11, 0.17, 0.25, 0.33, 0.42), and W, Mo-doped V/ZrO_2 materials with W or Mo/V atomic ratio = 0.66 were synthesized by adopting flame spray pyrolysis technique and investigated for the low-temperature SCR of NO with NH_3 in the presence of excess oxygen. The absence of crystalline vanadia and ZrV_2O_7 solid solution, as shown by the XRD measurements, indicates highly isolated state of dominant surface monomeric VO_x species in the V/ZrO_2 samples with V/Zr $\leq$ 0.17. Further increase in vanadia content led to

the formation of ZrV_2O_7 solid solution as a result of zirconia migration into the V_2O_5 crystallites. As a result, the number of adjacent oxygen coordination around V decreases substantially and results in the formation of new structure, the change in lattice parameter and crystal anisotropy can block the release of labile oxygen, and thus leads to the decrease in catalytic reduction of NO with NH_3. This finding is further supported by the dependence of the intrinsic SCR activity on the surface concentration of vanadia. The presence of surface monomeric VO_x species and doping with W^{6+} strongly enhances the reactive lattice oxygen content as well as potential site reducibility, which are evident by the H_2-TPR results. The highest surface reducibility was measured for 15V-WO_x(0.66)/ZrO_2 sample. The tungsten doping has a strong impact on the NO conversion, since tungsten loading with the W/V ratio = 0.66 exhibits a maximum conversion of ~98% in the temperature range 180–240 °C, whereas the molybdenum loading showed an inhibition effect on the SCR activity of V/ZrO_2 catalyst. When ammonia contacts with the surface of V/ZrO_2, the strong absorption peaks were observed in the in-situ FT-IR spectra which are attributed to the asymmetric and symmetric bending vibration mode of NH^{4+} bound to Brönsted acid sites have seen to decrease with respect to temperature. No gaseous N_2O species were detected at 2224 cm^{-1}, 1286 cm^{-1} in the in-situ FT-IR spectra of NO adsorbed over the V/ZrO_2. Our in-situ FT-IR and NH_3-TPD studies are evident for the direct correlation between the concentration of the Brönsted acid sites and SCR activity.

Acknowledgement

The authors wish to acknowledge financial support from the National Science Foundation (Grant No. NSF-0828226).

References

[1] B. Thirupathi, P.G. Smirniotis, Journal of Catalysis 288 (2012) 74–83.
[2] J.A. Dumesic, N.-Y. Topsøe, H. Topsoe, T. Slabiak, Journal of Catalysis 163 (1996) 409.
[3] N.-Y. Topsøe, Science 265 (1994) 1217–1219.
[4] G. Busca, L. Lietti, G. Ramis, F. Berti, Applied Catalysis B: Environmental 18 (1998) 1–36.
[5] J.G. Eon, R. Olier, J.C. Volta, Journal of Catalysis 145 (1994) 318.
[6] P. Ciambelli, L. Lisi, G. Russo, J.C. Volta, Applied Catalysis B: Environmental 7 (1995) 1.
[7] L.J. Lakshrni, K. Narshha, P. Kanta Rao, Applied Catalysis A 94 (1993) 61.
[8] V.K. Sharma, A. Wokaun, A. Baiker, Journal of Physical Chemistry 90 (1986) 2715.
[9] W.J. Stark, K. Wegner, S.E. Pratsinis, A. Baiker, Journal of Catalysis 197 (2001) 182–191.
[10] W.J. Stark, A. Baiker, S.E. Pratsinis, Particle and Particle Systems Characterization 19 (2002) 306–311.
[11] R. Jossen, M.C. Heine, S.E. Pratsinis, S.M. Augustine, M.K. Akhtar, Applied Catalysis B 69 (2007) 181–188.
[12] W.Y. Teoh, R. Amal, L. Mädler, S.E. Pratsinis, Catalysis Today 120 (2007) 203.
[13] K. Tanabe, Materials Chemistry and Physics 13 (1985) 347.
[14] M. Valigi, A. Chino, D. Cordischi, S. De Rossi, C. Ferrari, G. Ferraris, D. Gazzoli, V. Indovina, M. OcchiuzZi, Solid State Zonics 136 (1993) 63–65.
[15] S. Szakacs, G.J. Altena, T. Fransen, J.G. Van Ommen, J.R.H. Ross, Catalysis Today 16 (1993) 237.
[16] V. Indovina, M. Occhiuzzi, P. Ciambelli, D. Sannino, G. Ghiotti, F. Prinetto, in: J.W. Hightower, W.N. Delgass, E. Iglesia, A.T. Bell (Eds.), Proceedings of the 11th International Congress on Catalysis 40th Anniversary, Elsevier, Amsterdam, 1996, p. 691.
[17] I. Rossetti, L. Fabbrini, N. Ballarini, C. Oliva, F. Cavani, A. Cericola, B. Bonelli, M. Piumetti, E. Garrone, H. Dyrbeck, E.A. Blekkan, L. Forni, Journal of Catalysis 256 (2008) 45–61.
[18] V. Kumar, N. Lee, C.B. Almquist, Applied Catalysis B 69 (2006) 101–114.
[19] B.Z. Tian, C.Z. Li, F. Gu, H.B. Jiang, Y.J. Hu, J.L. Zhang, Chemical Engineering Journal 151 (2009) 220–227.
[20] P.M. Michalakos, H.E. Bellis, P. Brusky, H.H. Kung, H.Q. Li, W.R. Moser, W. Partenheimer, L.C. Satek, Industrial and Engineering Chemistry Research 34 (1995) 1994–2000.
[21] B. Schimmoeller, Y.J. Jiang, S.E. Pratsinis, A. Baiker, Journal of Catalysis 274 (2010) 64–75.
[22] W.Y. Teoh, R. Setiawan, L. Mädler, J.-D. Grunwaldt, R. Amal, S.E. Pratsinis, Chemistry of Materials 20 (2008) 4069.
[23] R. Kydd, W.Y. Teoh, K. Wong, Y. Wang, Q. Zeng, J. Scott, A. Yu, J. Zou, R. Amal, Advanced Functional Materials 19 (2009) 369.
[24] R. Koirala, G.K. Reddy, S.E. Pratsinis, P.G. Smirniotis, Journal of Physical Chemistry C 115 (2011) 24804–24812.
[25] J. Rack, S. Guk, Y. Il, S. Hayashi, Journal of Catalysis 159 (1996) 170–177.
[26] S. Su, A. Bell, Journal of Physical Chemistry B 102 (1998) 7000–7007.
[27] D. Gazzoli, S. Rossi, G. Ferraris, G. Mattei, R. Spinicci, M. Valigi, Journal of Molecular Catalysis A: Chemical 310 (2009) 17–23.
[28] W.J. Stark, K. Wegner, S.E. Pratsinis, A. Baiker, Journal of Catalysis 197 (2001) 182.
[29] B. Schimmoeller, H. Schulz, S.E. Pratsinis, A. Bareiss, A. Reitzmann, B.K. Czarnetzki, Journal of Catalysis 243 (2006) 82.
[30] S.A. Song, K.Y. Jung, S.B. Park, Langmuir 25 (2009) 3402–3406.
[31] R. Mueller, L. Mädler, S.E. Pratsinis, Chemical Engineering Science 58 (2003) 1969–1976.
[32] H.C. Chang, S.J. Kim, H.D. Jang, J.W. Choi, Colloids and Surfaces A: Physicochemical and Engineering Aspects 313 (2008) 282–287.
[33] S.E. Pratsinis, Progress in Energy and Combustion Science 24 (1998) 197.
[34] A.I.Y. Tok, F.Y.C. Boey, S.W. Du, B.K. Wong, Materials Science and Engineering B 130 (2006) 114.
[35] P.G.W.A. Kompio, A. Brückner, F. Hipler, G. Auer, E. Löffler, W. Grünert, Journal of Catalysis 286 (2012) 237–247.
[36] E.P. Reddy, R.S. Varma, Journal of Catalysis 221 (2004) 93–101.
[37] F. Orellana, J.P.D. Los Reyes, S. Urizar, Journal of the Chilean Chemical Society 48 (2003) N2.
[38] H. Bosch, B.J. Kip, J.G. van Ommen, P.J. Gellings, Journal of the Chemical Society, Faraday Transactions I 80 (1984) 2479.
[39] B. Schimmoeller, H. Schulz, A. Ritter, A. Reitzmann, B.K. Czarnetzki, A. Baiker, S.E. Pratsinis, Journal of Catalysis 256 (2008) 74–83.
[40] M.M. Koranne, J.G. Goodwin, G. Marcelin, Journal of Catalysis 148 (1994) 369–377.
[41] M. Inomata, A. Miyamoto, Y. Murakami, Journal of Physical Chemistry 85 (1981) 2372.
[42] J.S.O. Evans, J.C. Hanson, A.W. Sleight, Acta Crystallographica B54 (1998) 705–713.
[43] R.L. Withers, J.S.O. Evans, J. Hanson, A.W. Sleight, Journal of Solid State Chemistry 137 (1998) 161–167.
[44] Y. Yamamura, A. Horikoshi, S. Yasuzuka, H. Saitoh, K. Saito, Dalton Transactions 40 (2011) 224.
[45] M. Takagi, T. Kawai, M. Soma, O. Takaharu, K. Tamaru, Journal of Catalysis 50 (1977) 441.
[46] H.C. Yao, M. Shelef, in: R.L. Klimisch, J.G. Larsen (Eds.), Solid Electrolytes and their applications, Plenum, New York, 1975, p. 45.
[47] K. Otto, M. Shelef, Journal of Catalysis 14 (1969) 226.
[48] N.Y. Topsøe, H. Topsøe, J.A. Dumesic, Journal of Catalysis 151 (1995) 226–240.
[49] G. Ramis, G. Busca, F. Bregani, P. Forzatti, Applied Catalysis 64 (1990) 259.
[50] G. Ramis, G. Busca, F. Bregani, P. Forzatti, in: S. Yoshida, N. Takezawa, T. Ono (Eds.), Catalytic Science and Technology, vol. 1, Kondasha, Tokyo, 1991, p. 189.
[51] N.-Y. Topsøe, Journal of Catalysis 128 (1991) 499–511.
[52] Y. Chi, S.S.C. Chuang, Journal of Catalysis 190 (2000) 75–91.
[53] G. Busca, Langmuir 2 (1986) 577.
[54] K. Nakamoto, Infrared and Raman Spectra of Inorganic and Coordination Compounds, Wiley, New York, 1978.
[55] N.E. Tretyakov, V.N. Filimonov, Kinetics and Catalysis 14 (1973) 803.
[56] H. Matralis, M. Ciardelli, M. Ruwet, P. Grange, Journal of Catalysis 157 (1995) 523.
[57] G. Ramis, L. Yi, G. Busca, Catalysis Today 28 (1996) 373.
[58] N.-Y. Topsoe, H. Topsoe, Catalysis Today 9 (1991) 77.
[59] H. Schneider, S. Tschudin, M. Schneider, A. Wokaun, A. Baiker, Journal of Catalysis 147 (1994) 5–14.
[60] M. Kantcheva, Journal of Catalysis 204 (2001) 479–494.
[61] W.S. Kijlstra, D.S. Brands, E.K. Poels, A. Bliek, Journal of Catalysis 171 (1997) 208–218.